Published in final edited form as:
Curr Radiopharm. 2011 April 1; 4(2): 131–139.

PET Tracers Based on Zirconium-89

Yin Zhang[a], **Hao Hong**[b], and **Weibo Cai**[a,b,c,*]

[a]Department of Medical Physics, School of Medicine and Public Health, University of Wisconsin - Madison, Madison, Wisconsin, USA

[b]Department of Radiology, School of Medicine and Public Health, University of Wisconsin - Madison, Madison, Wisconsin, USA

[c]University of Wisconsin Carbone Cancer Center, Madison, Wisconsin, USA

Abstract

Positron emission tomography (PET) imaging with radiolabeled monoclonal antibodies has always been a dynamic area in molecular imaging. With decay half-life (3.3 d) well matched to the circulation half-lives of antibodies (usually on the order of days), ^{89}Zr has been extensively studied over the last decade. This review article will give a brief overview on ^{89}Zr isotope production, the radiochemistry generally used for ^{89}Zr-labeling, and the PET tracers that have been developed using ^{89}Zr. To date, ^{89}Zr-based PET imaging has been investigated for a wide variety of cancer-related targets, which include human epidermal growth factor receptor 2, epidermal growth factor receptor, prostate-specific membrane antigen, splice variant v6 of CD44, vascular endothelial growth factor, carbonic anhydrase IX, insulin-like growth factor 1 receptor, among others. With well-developed radiochemistry, commercial availability of chelating agents for ^{89}Zr labeling, increasingly widely available isotope supply, as well as successful proof-of-principle in pilot human studies, it is expected that PET imaging with ^{89}Zr-based tracers will be a constantly evolving and highly vibrant field in the near future.

Keywords

Zirconium-89 (^{89}Zr); positron emission tomography (PET); molecular imaging; radioimmunoPET; monoclonal antibody (mAb); cancer

INTRODUCTION

Radiolabeled antibodies have been used in the clinic for diagnostic and therapeutic purposes for over 40 years [1-3]. The use of radiolabeled antibodies as imaging probes to visualize tumors has always been a vibrant area in molecular imaging. In particular, positron emission tomography (PET) with radiolabeled monoclonal antibodies (mAbs), sometimes termed as “immunoPET”, is an attractive method for non-invasive tumor detection since this strategy combines the high sensitivity of PET with the high antigen specificity of mAbs. If the mAb is used for systemic therapy of cancer (either as a single agent or in combination with other anti-cancer drugs), immunoPET with the radiolabeled mAb can be used for tumor detection as well as treatment planning.

*Requests for reprints: Weibo Cai, PhD, Departments of Radiology and Medical Physics, School of Medicine and Public Health, University of Wisconsin - Madison, 1111 Highland Ave, Room 7137, Madison, WI 53705-2275, USA. wcai@uwhealth.org; Fax: 1-608-265-0614; Tel: 1-608-262-1749. .

Among the more than 100 PET isotopes, the majority are not suitable for PET imaging applications because of undesirable decay half-life, poor availability, high production cost, underdeveloped radiochemistry, among others. Within the commonly used PET isotopes, only a few of them are suitable for antibody labeling since immunoPET requires that the PET isotope can be attached to the mAb with good in vivo stability and the decay half-life of the isotope should match the pharmacokinetics of the mAb. Currently, some of the commonly used PET isotopes for antibody labeling include ^{89}Zr ($t_{1/2}$ = 3.3 d), ^{124}I ($t_{1/2}$ = 4.2 d), ^{64}Cu ($t_{1/2}$ = 12.7 h), ^{86}Y ($t_{1/2}$ = 14.7 h), among others. This review article will summarize the current status of PET tracers based on ^{89}Zr.

Zirconium is a transition metal in Group IVB of the periodic table. ^{89}Zr, which decays by positron emission (23%) and electron capture (77%) to the stable isotope ^{89}Y, has attractive characteristics for immunoPET applications. The physical decay half-life of ^{89}Zr is 3.3 days, which is compatible with the time needed to achieve optimal tumor-to-background ratios for intact mAbs (typically a few days). The E_{max} of 897 keV and E_{ave} of 396.9 keV for its positron emission, lower than that of ^{124}I (which has a similar decay half-life), could result in PET images with good spatial resolution. Ideally, a positron emitter should not have prompt photons with energy near 511 keV in order to achieve better quantitative accuracy. The spontaneous gamma decay of ^{89}Zr gives rise to 908.97 keV photons (99% abundance), which can be easily gated off by setting the energy window of a PET scanner.

There are several advantages of using ^{89}Zr over other PET isotopes with comparable decay half-lives such as ^{124}I. For example, there is no need to use highly enriched target and the energy required for ^{89}Zr production is lower [4]. ^{124}I linked directly to mAbs via tyrosine residues can be subjected to dehalogenation in vivo, which can lead to significant radioactivity uptake in non-targeted organs unrelated to mAb-antigen binding [5]. In addition, if the mAb undergoes internalization after binding to its target, lysosomal proteolysis of the mAb generally results in rapid loss of ^{124}I from the cell but accumulation of radiometals such as ^{89}Zr [6]. The major disadvantages of ^{89}Zr include limited availability and the high energy gamma emission at 908.97 keV, which may limit the radioactive dose that can be administered into patients.

PRODUCTION OF ^{89}Zr

^{89}Zr can be produced via either ^{89}Y(p,n)^{89}Zr or ^{89}Y(d,2n)^{89}Zr reaction [7-12]. The chemistry for separating ^{89}Zr from the target is the same independent of the production method. In a typical ^{89}Y(p,n)^{89}Zr reaction, proton beam with 14-14.5 MeV energy is used to bombard inexpensive natural yttrium foil mounted onto an aluminum/copper disc for 2-3 h (65-80 μA) and isotope separation is done via ion exchange chromatography or solvent extraction after bombardment. With optimal irradiation time, this method can lead to < 0.2% impurity level of ^{88}Zr [4]. Alternatively, the ^{89}Y(d,2n)^{89}Zr reaction can be used to minimize the level of ^{88}Zr. Yttrium pellet is irradiated with a 16 MeV deuteron beam and ^{89}Zr can be separated from the target by ion exchange chromatography with an overall yield of ~80% [12]. The impurity level of ^{88}Zr can be kept as low as 0.008% at the end of bombardment. Although the yield of the ^{89}Y(d,2n)^{89}Zr reaction can be improved by using higher energy deuteron beam, the impurity level of ^{88}Zr may also be higher. The radionuclidic purity of the product can be determined by gamma spectroscopy, where a germanium detector is coupled to a multichannel analyzer. Currently, high specific activity ^{89}Zr (typically in the form of ^{89}Zr-chloride) can be produced by several facilities around the world, which can be shipped to remote sites [13].

RADIOLABELING OF ^{89}Zr

^{89}Zr labeling of antibodies can be achieved through various types of chelators, primarily desferrioxamine B (Df) which can form a stable chelate with ^{89}Zr through the 3 hydroxamate groups [14]. A representative route for ^{89}Zr-labeling is shown in Fig. (1A). Generally, mAbs are conjugated with a bifunctional derivative of Df via an amide linkage for subsequent labeling with ^{89}Zr [15]. The hydroxamate groups within Df need to be temporarily blocked with Fe(III) before mAb conjugation. Subsequently, Fe(III) is removed by transchelation to ethylenediaminetetraacetic acid (EDTA) before the conjugate is exposed to ^{89}Zr. The choice of Df as the chelator for ^{89}Zr is attractive because it has been safely used in the clinic for many years. In the past and ongoing clinical studies, neither adverse reactions nor significant changes in blood and urine values were observed after injection of Df-containing conjugates. Moreover, no antibody responses directed against the Df chelate were observed, indicating that its immunogenicity is quite low [16].

Despite the success of this strategy, the multi-step procedure is quite complicated and time-consuming which makes it challenging to produce ^{89}Zr-labeled mAbs in compliance to the current Good Manufacturing Practice (cGMP) for clinical investigations. Recently, a new bifunctional chelate was reported for ^{89}Zr labeling: *p*-isothiocyanatobenzyl-desferrioxamine B (Df-Bz-NCS) [17]. As shown in Fig. (1B), labeling of ^{89}Zr has been significantly simplified into a 2-step procedure (the initial strategy has 6 steps) [18]. Coupling of Df-Bz-NCS to mAbs was very efficient and it has been reported that a reproducible chelate:mAb ratio of 1.5:1 could be obtained using only a three-fold molar excess of Df-Bz-NCS [17]. Such a low chelate:mAb ratio can avoid alteration of the pharmacokinetics or immunoreactivity of the mAb. Comparing the 2 strategies, the rate of ^{89}Zr complexation was very similar, indicating that different chemical linkages (e.g. S instead of O in the side chain which might be involved in $^{89}Zr^{4+}$ coordination) have little influence on the radiochemistry. At the optimal pH (7.0), almost quantitative complexation was achieved after 30 min incubation at room temperature, with no impairment of the immunoreactivity of the mAbs.

The need for protection of radioimmunoconjugates against radiation damage during storage has been demonstrated in various studies [9,19]. The presence of the antioxidant ascorbic acid during storage of high-dose ^{90}Y/^{131}I-labeled mAbs has been proven to be beneficial. However, ascorbic acid cannot be used for storage of ^{89}Zr-labeled mAbs since it can cause detachment of ^{89}Zr from Df by reducing Zr^{4+} to Zr^{2+} [9]. It was suggested that ^{89}Zr-Df-Bz-NCS-mAb can be best stored at 4 °C in sodium acetate buffer in presence of the antioxidant gentisic acid. It is worth noting that under certain storage conditions, the ^{89}Zr-Df-Bz-NCS-mAb conjugate is slightly less stable than the conjugate obtained from the 6-step strategy. In particular, the presence of Cl^- in the storage buffer can impair the integrity of the radioimmunoconjugates. This is likely due to radiation-induced formation of OCl^- which can react with the thiol group of the enolised thiourea unit, which in turn can lead to a series of events such as coupling reactions and cleavage of methionyl peptide bonds.

Besides the two abovementioned methods, the reaction between N-(S-acetyl)thioacetyl-Df (SATA-Df) and maleimide-conjugated mAb was also investigated [20,21]. However, the resulting conjugates were found to be unstable in human serum at 37°C [9]. Recently, several thiol-reactive Df ligands were tested for labeling mAbs in a site-specific manner [22], using engineered mAbs containing selectively positioned cysteine residues. In this study, the amino group of Df was acylated by various chemicals to obtain thiol-reactive reagents bromoacetyl-desferrioxamine (Df-Bac), iodoacetyl-desferrioxamine (Df-Iac) and maleimidocyclohexyl-desferrioxamine (Df-Chx-Mal), respectively. Df-Bac and Df-Iac alkylated the thiol groups of thio-trastuzumab by nucleophilic substitution, while Df-Chx-

Mal led to the conjugate Df-Chx-Mal-thio-trastuzumab. Each Df-modified thio-trastuzumab conjugate was labeled with ^{89}Zr in high yield and the resulting tracers exhibited good tumor-to-blood ratio in a breast cancer model.

PET IMAGING WITH ^{89}Zr

To date, a wide variety of mAbs have been labeled with ^{89}Zr and several of these ^{89}Zr-labeled mAbs have entered clinical investigation with promising results. With wider availability of ^{89}Zr and simpler chemistry for radiolabeling, it is expected that more and more PET tracers based on ^{89}Zr will be developed in the coming years.

Imaging HER2

Human epidermal growth factor receptor 2 (HER2), a member of the ErbB tyrosine kinase receptor family, is involved in cell survival, differentiation, proliferation, metastasis, and angiogenesis [23-25]. Overexpression of HER2 has been found in a wide variety of human cancers. Currently, HER2 overexpression is determined using immunohistochemistry and fluorescence *in situ* hybridization (FISH) at the time of diagnosis of the primary tumor. Non-invasive imaging of HER2 expression and localization of HER2-overexpressing tumor lesions using immunoPET could be a practical method in the clinic to guide HER2-targeted therapy.

Trastuzumab (i.e. Herceptin), an anti-HER2 mAb that was approved by the Food and Drug Administration (FDA) to treat HER2-positive breast cancer, has been extensively investigated for imaging applications over the last decade [23,24]. In one study, clinical-grade ^{89}Zr-trastuzumab was developed for potential clinical immunoPET imaging applications [26]. In nude mice bearing HER2-positive tumors, ^{89}Zr-trastuzumab exhibited excellent tumor uptake (~30%ID/g) with high tumor-to-nontumor ratios. The biodistribution pattern of ^{89}Zr-trastuzumab was similar to that of ^{111}In-trastuzumab, which was reported in a previous clinical study [27]. In addition, ^{89}Zr-trastuzumab was very stable in both buffer solutions and human serum.

The ability of ^{89}Zr-trastuzumab PET to quantify the alternations in HER2 expression level after treatment with a heat shock protein 90 (Hsp90) inhibitor has been investigated [28]. PET imaging revealed significant decrease of tracer uptake in the tumor, indicating that ^{89}Zr-trastuzumab PET can be employed for non-invasive quantification of HER2 down-regulation after treatment. Similar findings were also observed in a separate study using a differently labeled ^{89}Zr-trastuzumab and a different Hsp90 inhibitor [29]. Recently, site-specific labeling of engineered trastuzumab (through cysteine residues) with ^{89}Zr was reported [22]. The resulting tracers were stable in serum and showed PET imaging properties comparable to conventionally prepared ^{89}Zr-trastuzumab, where labeling was achieved through the lysine residues.

First-in-human study of ^{89}Zr-labeled trastuzumab for PET imaging of HER2-positive lesions has been reported [30]. The tracer showed excellent tumor uptake which allowed detection of most of the known lesions and, more importantly, some lesions that had not been detected earlier (Fig. (2)). Interestingly, the dose of trastuzumab for optimal PET imaging performance was chosen to be 37 MBq of ^{89}Zr-trastuzumab in a total of 50 mg protein for trastuzumab-naive patients or 10 mg protein for patients that are already on trastuzumab treatment. The exact mechanisms underlying such dose-dependent pharmacokinetics of ^{89}Zr-trastuzumab are not known. One possible explanation is that it involves rapid but saturable elimination of low doses from the circulation during the first elimination phase, which has a half-life of ~4 days. Another mechanism that may play a role in increasing ^{89}Zr-trastuzumab clearance in trastuzumab-naive patients is the presence of high plasma levels of

extracellular domains shed by HER2. After trastuzumab (or ^{89}Zr-trastuzumab) binds to these extracellular domains, the resulting complex is cleared by the liver and excreted into the intestines.

Recently, another study indicated that trastuzumab pharmacokinetics and organ distribution can also be heavily affected by an extensive tumor load [31]. Therefore, a study with a more patient-tailored trastuzumab dosing schedule on the basis of tumor volume in addition to bodyweight should be considered in the future. However, one needs to bear in mind that such dose-dependent pharmacokinetics may not be applicable to ^{89}Zr-labeled antibodies which bind to other cancer-related targets.

Imaging EGFR

The epidermal growth factor receptor (EGFR), another member of the ErbB family, is a 170 kDa protein which plays a critical role in tumor cell proliferation, differentiation, and survival [23,32]. EGFR overexpression has been associated with a number of cancers such as breast carcinoma, lung cancer, bladder cancer, and colon carcinoma [25,33]. In addition, EGFR expression is often associated with more aggressive tumors, poor prognosis, and resistance to treatment with cytotoxic agents. Therefore, EGFR is one of the most extensively studied targets in oncology and many mAbs have been developed against EGFR for cancer therapy [34].

Cetuximab (Erbitux, ImClone System Inc.) is a chimeric IgG1 mAb that can block EGFR activation by binding to the ligand-binding domain, which induces internalization of EGFR thereby preventing downstream signaling [35]. ^{89}Zr-labeled cetuximab has been investigated in several preclinical studies [36,37]. In one early report, ^{89}Zr-cetuximab PET was used as a scouting procedure before radioimmunotherapy (RIT) to confirm tumor targeting and allow estimation of radiation dose delivery to tumors and normal tissues [36]. It was concluded that ^{89}Zr-cetuximab could serve as a surrogate for scouting the biodistribution of ^{90}Y-cetuximab and ^{177}Lu-cetuximab in tumor-bearing mice.

In another study, disparity between in vivo EGFR expression level and ^{89}Zr-cetuximab uptake in the tumors was observed in mouse models, suggesting that additional pharmacokinetic or pharmacodynamic mechanisms may influence the tumor uptake of cetuximab as well as the therapeutic efficacy of this agent [37]. It was suggested that these additional mechanisms may explain why receptor expression levels alone are not sufficient to predict patient response to anti-EGFR therapies. Various studies have revealed that a majority of tumors responding to EGFR kinase inhibitors harbor activating mutations in the EGFR kinase domain [38]. Therefore, imaging of EGFR mutant expression might be more useful in selecting the right patient population for personalized treatment as well as predicting the therapeutic response [39].

Imaging PSMA

The prostate-specific membrane antigen (PSMA), a 100 kDa type II transmembrane glycoprotein, is one of the best characterized targets in oncology [40]. PSMA expression levels have been shown to exhibit a positive correlation with increased tumor progression, development of castration resistance, and/or resistance to hormone-based therapies. Although PSMA expression has also been detected in a limited range of normal tissues including benign prostatic epithelium, renal proximal tubule, small bowel, and the brain, these normal tissue sites only express PSMA at levels 2-3 orders of magnitude lower than that observed in more than 95% of clinical prostate cancer specimens [41]. In addition, expression of PSMA in normal tissues is highly polarized to the apical or luminal sides of

various tissues which are not readily accessible to circulating mAbs, thus making anti-PSMA mAbs functionally tumor-specific.

In a recent study, a ^{89}Zr-labeled anti-PSMA mAb, J591, was reported for immunoPET and quantification of PSMA expression in vivo [42]. PET imaging of male athymic nude mice bearing subcutaneous LNCaP (PSMA-positive) or PC-3 (PSMA-negative) tumors was conducted and ^{89}Zr-J591 provided excellent image contrast for delineating the LNCaP xenografts at a few days after tracer administration, which may potentially be used in the clinic to non-invasively identify and quantify PSMA-positive prostate tumors in patients. Interestingly, a "multimodality" approach to image PSMA expression has also been carried out using ^{89}Zr-J591 [43]. Taken advantage of the phenomenon known as the Cerenkov effect (the emission of light from a transparent substance when a charged particle, such as an electron, travels through the material with a speed faster than the speed of light in that material), Cerenkov luminescence imaging (CLI) of tumors in vivo, using a small animal optical scanner, was carried out. The results obtained from optical scans correlated well with those obtained from immunoPET studies in a quantitative manner (Fig. (3)). Since CLI can be used to image radionuclides that do not emit either positrons or γ-rays and are thereby unsuitable for use with current nuclear imaging modalities, it may serve as a potential new imaging modality for rapid and high-throughput screening of radiopharmaceuticals.

Imaging CD44v6

CD44 is a cell-surface glycoprotein involved in a wide variety of biological processes such as lymphocyte-endothelial cell interactions, adhesion of cells to extracellular matrix proteins, lymphohematopoiesis, homotypic adhesion, T cell activation/adherence, cytokine release, metastasis formation, and lateral movement of cells [44,45]. The CD44 protein family is composed of several isoforms, encoded by standard exons and many alternatively spliced variant exons, which are expressed in a tissue-specific manner. The splice variant v6 of CD44 (denoted as "CD44v6") has been implicated in tumorigenesis, tumor cell invasion, and metastasis [46,47]. Although CD44v6 is expressed only in a subset of normal epithelial tissues (e.g. thyroid and prostate glands), homogeneous expression of CD44v6 has been found in various solid tumor types such as squamous cell carcinoma of the head and neck (HNSCC), lung, skin, esophageal, and cervical cancer [48]. In addition, heterogeneous expression of CD44v6 has been found in adenocarcinomas of the breast, lung, colon, pancreas, and stomach.

In order to avoid human antimouse immune responses, the chimeric IgG_1 derivative of a murine mAb (U36 which binds to CD44v6) was constructed. ^{186}Re-labeled chimeric mAb (cmAb), termed as "cU36", was then tested in phase I trials which showed promising anti-tumor effects in patients with HNSCC [49,50]. Subsequently, ^{89}Zr-labeled cU36 was investigated in xenograft-bearing mice [9]. Further, ^{89}Zr-cU36 was also tested for the first time in HNSCC patients who were at high risk of having neck lymph node metastases [16]. Serial PET scans after injection of 2.0 mCi of ^{89}Zr-cU36 successfully detected the primary head and neck tumors as well as metastases in the neck, with sensitivity at least as good as computed tomography (CT) or magnetic resonance imaging (MRI). However, a few patients developed an antibody response directed against cU36 although no evidence was found for antibody reactions against the chelate. In addition, ^{89}Zr-cU36 was not able to detect micrometastases in patients, similar to the findings of a previous biodistribution study with the mAb U36 [51]. In another study of cU36, it was reported that ^{89}Zr-labeled mAbs are more suitable for scouting of therapeutic doses of ^{90}Y-labeled mAbs while ^{124}I-labeled mAbs are better for scouting of ^{131}I- and ^{186}Re-labeled mAbs [52].

Radiation dosimetry estimation in patients injected with ^{89}Zr-cU36 revealed that ^{89}Zr-cU36 was safe and well-tolerated in all patients [53]. Although the mean radiation dose for

patients in this study was estimated to be around 40 mSv, which would limit repeated application of ^{89}Zr immunoPET, the constant improvement of new clinical PET/CT scanners may allow the acquisition of better-quality PET images with a lower injected radioactivity dose. In a recent study, different ^{89}Zr-labeling chemistry (i.e. the 2-step and 6-step methods; Fig. (1)) was compared for cU36 in a mouse model [17]. High level accumulation of ^{89}Zr-labeled cU36 in the tumors and low level of tracer uptake in normal tissues were observed for both tracers.

Imaging VEGF

Vascular endothelial growth factor (VEGF), a potent mitogen in embryonic and somatic angiogenesis, plays a pivotal role in both normal vascular tissue development and many disease processes such as tumor development and metastasis [54]. Overexpression of VEGF and/or VEGF receptors (VEGFRs) has been implicated as a marker of poor prognosis in various clinical studies [55]. The humanized anti-VEGF mAb, bevacizumab (i.e. Avastin), can block VEGF-induced tumor angiogenesis and was approved by the FDA to treat multiple metastatic cancers [56].

In 2007, ^{89}Zr-labeled bevacizumab was investigated in nude mice bearing human ovary cancer SKOV-3 xenograft tumors [57]. Comparing ^{89}Zr-bevacizumab and ^{89}Zr-IgG, which served as a control, PET showed uptake of ^{89}Zr-bevacizumab in well-perfused organs at 24 h post-injection and clear tumor localization after 72 h. The uptake of ^{89}Zr-bevacizumab was significantly higher than that of ^{89}Zr-IgG, suggesting target specificity of the tracer. Recently, ^{89}Zr-bevacizumab was also successfully used to detect the early anti-angiogenic tumor response to treatment with a Hsp90 inhibitor (Fig. (4)), indicating that ^{89}Zr-bevacizumab PET can be a sensitive and non-invasive technique for monitoring the anti-tumor effect [58].

Imaging Other Targets

Besides the abovementioned targets, several other proteins have also been investigated using ^{89}Zr-based PET. Hypoxic tumor cells are resistant to radiotherapy and various chemotherapeutic agents. Carbonic anhydrase IX (CAIX), an endogenous hypoxia-related protein, is upregulated in many tumor types [59]. Therefore, pre-therapeutic assessment of intratumoral hypoxia may allow selection of patients for intensified treatment regimens. Recently, ^{89}Zr-labeled cG250-F(ab')$_2$, an anti-CAIX antibody fragment, was shown to allow visualization of tumor hypoxia with PET in a xenograft tumor model, which correlated spatially to the microscopic distribution of CAIX-expressing cells [60]. This study suggested a potential role of ^{89}Zr-cG250-F(ab')$_2$ for non-invasive imaging of hypoxia in head and neck carcinomas, which deserves further exploration in the future.

In one report, expression of the insulin-like growth factor 1 receptor (IGF1R) was measured by PET with ^{89}Zr-labeled R1507, a mAb against IGF1R [61]. Excellent contrast and prominent tracer uptake in the tumor was observed in mouse bearing triple-negative breast cancer tumors, which may enable future patient selection for IGF1R-targeted therapy in the clinic since currently there is no effective therapeutic regimes for this sub-population of breast cancer patients.

Single-walled carbon nanotubes (SWCNTs) have unique properties which make them suitable for applications in a wide variety of imaging modalities, such as MRI, near-infrared fluorescence, Raman spectroscopy, photoacoustic tomography, and radionuclide-based imaging [62,63]. Recently, SWCNTs were conjugated to E4G10, an antibody specifically binds to the monomeric vascular endothelial cadherin (VE-cad) epitope expressed in angiogenic tumor vessels, and labeled with ^{89}Zr [64]. Dynamic and longitudinal PET

imaging of this agent in LS174T human colorectal tumor-bearing mice demonstrated rapid blood clearance and target-specific tumor accumulation. Due to the large surface areas of SWCNTs, a single construct could be designed to incorporate both imaging and therapeutic agents onto the same platform. In addition, since VE-cad is expressed by the tumor vasculature, it was suggested that a single agent may potentially be employed to image or treat a variety of different tumors types.

CONCLUSIONS

Over the last several years, PET imaging with ^{89}Zr-based agents has been a highly dynamic research area. To date, the majority of agents that have been labeled with ^{89}Zr are mAbs, because the decay half-life of ^{89}Zr matches very well with the biological half-life of antibodies. While this manuscript was in preparation, PET imaging of integrin $\alpha_v\beta_3$ expression using ^{89}Zr-labeled arginine-glycine-aspartic acid (RGD) peptides were reported [65]. Although efficient radiolabeling of peptides with ^{89}Zr was achieved and the tracer gave good PET images in xenograft models, it was concluded that labeling peptides with ^{89}Zr is not optimal due to the relatively rapid clearance of peptide tracers from the tumor region, as well as the increased bone uptake of transchelated ^{89}Zr over time. Therefore, it appears that the most promising applications of ^{89}Zr are for the labeling and PET imaging of long-circulating agents such as mAbs and certain nanoparticles.

Currently, labeling of ^{89}Zr is primarily through desferrioxamine B which serves as the chelator. Based on the available literature data, the ^{89}Zr-Df conjugate is quite stable for in vivo applications. Therefore, the key to in vivo stability of ^{89}Zr-based tracers lies in the linkage between Df and the antibody or the nanoparticle. Although site-specific labeling of ^{89}Zr will not compromise the immunoreactivity of the resulting antibody conjugate, while labeling through the lysine side chains of mAbs may (even though the number of Df groups per antibody is quite low), the requirement of protein engineering expertise will limit the wide-spread adoption of such site-specific labeling strategy.

With significantly simplified radiochemistry (i.e. the 2-step method), commercially available chelating agents for ^{89}Zr labeling, increasingly widely available isotope supply, as well as successful proof-of-principle in pilot human studies, it is expected that PET imaging with ^{89}Zr-based tracers will be a constantly evolving and highly vibrant field for the next decade. Much further efforts are needed to accelerate the translation of more promising ^{89}Zr-based tracers into clinical use.

Acknowledgments

This work is supported, in part, by the Wisconsin Partnership Program, the University of Wisconsin Carbone Cancer Center, a Susan G. Komen Postdoctoral Fellowship, and a DOD PCRP IDEA Award.

REFERENCES

[1]. Goldenberg DM, Sharkey RM. Advances in cancer therapy with radiolabeled monoclonal antibodies. Q. J. Nucl. Med. Mol. Imaging. 2006; 50:248–264. [PubMed: 17043623]

[2]. Goldenberg DM, Sharkey RM. Novel radiolabeled antibody conjugates. Oncogene. 2007; 26:3734–3744. [PubMed: 17530026]

[3]. McCardle RJ, Harper PV, Spar IL, Bale WF, Andros G, Jiminez F. Studies with iodine-131-labeled antibody to human fibrinogen for diagnosis and therapy of tumors. J. Nucl. Med. 1966; 7:837–847. [PubMed: 5955363]

[4]. Nayak TK, Brechbiel MW. Radioimmunoimaging with longer-lived positron-emitting radionuclides: potentials and challenges. Bioconjug. Chem. 2009; 20:825–841. [PubMed: 19125647]

[5]. Koehler L, Gagnon K, McQuarrie S, Wuest F. Iodine-124: a promising positron emitter for organic PET chemistry. Molecules. 2010; 15:2686–2718. [PubMed: 20428073]

[6]. Lee FT, Scott AM. Immuno-PET for tumor targeting. J. Nucl. Med. 2003; 44:1282–1283. [PubMed: 12902419]

[7]. Tang L. Radionuclide production and yields at Washington University School of Medicine. Q. J. Nucl. Med. Mol. Imaging. 2008; 52:121–133. [PubMed: 18043542]

[8]. Lewis JS, Welch MJ, Tang L. Workshop on the production, application and clinical translation of "non-standard" PET nuclides: a meeting report. Q. J. Nucl. Med. Mol. Imaging. 2008; 52:101–106. [PubMed: 18043544]

[9]. Verel I, Visser GW, Boellaard R, Stigter-van Walsum M, Snow GB, van Dongen GA. ^{89}Zr immuno-PET: comprehensive procedures for the production of ^{89}Zr-labeled monoclonal antibodies. J. Nucl. Med. 2003; 44:1271–1281. [PubMed: 12902418]

[10]. Pagani M, Stone-Elander S, Larsson SA. Alternative positron emission tomography with non-conventional positron emitters: effects of their physical properties on image quality and potential clinical applications. Eur. J. Nucl. Med. 1997; 24:1301–1327. [PubMed: 9323273]

[11]. Dejesus OT, Nickles RJ. Production and purification of ^{89}Zr, a potential PET antibody label. Int. J. Radiat. Appl. Instrum., A, Appl. Radiat. Isot. 1990; 41:789–790.

[12]. Zweit J, Downey S, Sharma HL. Production of no-carrier-added zirconium-89 for positron emission tomography. Int. J. Radiat. Appl. Instrum., A, Appl. Radiat. Isot. 1991; 42:199–201.

[13]. Holland JP, Sheh Y, Lewis JS. Standardized methods for the production of high specific-activity zirconium-89. Nucl. Med. Biol. 2009; 36:729–739. [PubMed: 19720285]

[14]. Meijs WE, Herscheid JDM, Haisma HJ, Pinedo HM. Evaluation of desferal as a bifunctional chelating agent for labeling antibodies with Zr-89. Int. J. Radiat. Appl. Instrum., A, Appl. Radiat. Isot. 1992; 43:1443–1447.

[15]. Herscheid JD, Hoekstra A, Vos CM. N-Succinyldesferrioxamine B: a potential radiopharmaceutical for assessing renal function. Eur. J. Nucl. Med. 1984; 9:508–510. [PubMed: 6549165]

[16]. Borjesson PK, Jauw YW, Boellaard R, de Bree R, Comans EF, Roos JC, Castelijns JA, Vosjan MJ, Kummer JA, Leemans CR, Lammertsma AA, van Dongen GA. Performance of immuno-positron emission tomography with zirconium-89-labeled chimeric monoclonal antibody U36 in the detection of lymph node metastases in head and neck cancer patients. Clin. Cancer Res. 2006; 12:2133–2140. [PubMed: 16609026]

[17]. Perk LR, Vosjan MJ, Visser GW, Budde M, Jurek P, Kiefer GE, van Dongen GA. p-Isothiocyanatobenzyl-desferrioxamine: a new bifunctional chelate for facile radiolabeling of monoclonal antibodies with zirconium-89 for immuno-PET imaging. Eur. J. Nucl. Med. Mol. Imaging. 2010; 37:250–259. [PubMed: 19763566]

[18]. Vosjan MJ, Perk LR, Visser GW, Budde M, Jurek P, Kiefer GE, van Dongen GA. Conjugation and radiolabeling of monoclonal antibodies with zirconium-89 for PET imaging using the bifunctional chelate p-isothiocyanatobenzyl-desferrioxamine. Nat. Protoc. 2010; 5:739–743. [PubMed: 20360768]

[19]. Chakrabarti MC, Le N, Paik CH, De Graff WG, Carrasquillo JA. Prevention of radiolysis of monoclonal antibody during labeling. J Nucl Med. 1996; 37:1384–1388. [PubMed: 8708780]

[20]. Meijs WE, Haisma HJ, Klok RP, van Gog FB, Kievit E, Pinedo HM, Herscheid JD. Zirconium-labeled monoclonal antibodies and their distribution in tumor-bearing nude mice. J. Nucl. Med. 1997; 38:112–118. [PubMed: 8998164]

[21]. Meijs WE, Haisma HJ, Van der Schors R, Wijbrandts R, Van den Oever K, Klok RP, Pinedo HM, Herscheid JD. A facile method for the labeling of proteins with zirconium isotopes. Nucl. Med. Biol. 1996; 23:439–448. [PubMed: 8832698]

[22]. Tinianow JN, Gill HS, Ogasawara A, Flores JE, Vanderbilt AN, Luis E, Vandlen R, Darwish M, Junutula JR, Williams SP, Marik J. Site-specifically ^{89}Zr-labeled monoclonal antibodies for ImmunoPET. Nucl. Med. Biol. 2010; 37:289–297. [PubMed: 20346868]

[23]. Cai W, Niu G, Chen X. Multimodality imaging of the HER-kinase axis in cancer. Eur. J. Nucl. Med. Mol. Imaging. 2008; 35:186–208. [PubMed: 17846765]

[24]. Niu G, Cai W, Chen X. Molecular imaging of human epidermal growth factor receptor 2 (HER-2) expression. Front. Biosci. 2008; 13:790–805. [PubMed: 17981588]

[25]. Gross ME, Shazer RL, Agus DB. Targeting the HER-kinase axis in cancer. Semin. Oncol. 2004; 31:9–20. [PubMed: 15052539]

[26]. Dijkers EC, Kosterink JG, Rademaker AP, Perk LR, van Dongen GA, Bart J, de Jong JR, de Vries EG, Lub-de Hooge MN. Development and characterization of clinical-grade 89Zr-trastuzumab for HER2/neu immunoPET imaging. J Nucl Med. 2009; 50:974–981. [PubMed: 19443585]

[27]. Perik PJ, Lub-De Hooge MN, Gietema JA, van der Graaf WT, de Korte MA, Jonkman S, Kosterink JG, van Veldhuisen DJ, Sleijfer DT, Jager PL, de Vries EG. Indium-111-labeled trastuzumab scintigraphy in patients with human epidermal growth factor receptor 2-positive metastatic breast cancer. J. Clin. Oncol. 2006; 24:2276–2282. [PubMed: 16710024]

[28]. Oude Munnink TH, Korte MA, Nagengast WB, Timmer-Bosscha H, Schroder CP, Jong JR, Dongen GA, Jensen MR, Quadt C, Hooge MN, Vries EG. ^{89}Zr-trastuzumab PET visualises HER2 downregulation by the HSP90 inhibitor NVP-AUY922 in a human tumour xenograft. Eur. J. Cancer. 2010; 46:678–684. [PubMed: 20036116]

[29]. Holland JP, Caldas-Lopes E, Divilov V, Longo VA, Taldone T, Zatorska D, Chiosis G, Lewis JS. Measuring the pharmacodynamic effects of a novel Hsp90 inhibitor on HER2/neu expression in mice using Zr-DFO-trastuzumab. PLoS One. 2010; 5:e8859. [PubMed: 20111600]

[30]. Dijkers EC, Oude Munnink TH, Kosterink JG, Brouwers AH, Jager PL, de Jong JR, van Dongen GA, Schroder CP, Lub-de Hooge MN, de Vries EG. Biodistribution of ^{89}Zr-trastuzumab and PET imaging of HER2-positive lesions in patients with metastatic breast cancer. Clin. Pharmacol. Ther. 2010; 87:586–592. [PubMed: 20357763]

[31]. Oude Munnink TH, Dijkers EC, Netters SJ, Lub-de Hooge MN, Brouwers AH, Haasjes JG, Schroder CP, de Vries EG. Trastuzumab pharmacokinetics influenced by extent human epidermal growth factor receptor 2-positive tumor load. J. Clin. Oncol. 2010; 28:e355–356. [PubMed: 20458048]

[32]. Normanno N, De Luca A, Bianco C, Strizzi L, Mancino M, Maiello MR, Carotenuto A, De Feo G, Caponigro F, Salomon DS. Epidermal growth factor receptor (EGFR) signaling in cancer. Gene. 2006; 366:2–16. [PubMed: 16377102]

[33]. Mitsudomi T, Yatabe Y. Epidermal growth factor receptor in relation to tumor development: EGFR gene and cancer. FEBS J. 2010; 277:301–308. [PubMed: 19922469]

[34]. Herbst RS, Shin DM. Monoclonal antibodies to target epidermal growth factor receptor-positive tumors: a new paradigm for cancer therapy. Cancer. 2002; 94:1593–1611. [PubMed: 11920518]

[35]. Goldstein NI, Prewett M, Zuklys K, Rockwell P, Mendelsohn J. Biological efficacy of a chimeric antibody to the epidermal growth factor receptor in a human tumor xenograft model. Clin. Cancer Res. 1995; 1:1311–1318. [PubMed: 9815926]

[36]. Perk LR, Visser GW, Vosjan MJ, Stigter-van Walsum M, Tijink BM, Leemans CR, van Dongen GA. ^{89}Zr as a PET surrogate radioisotope for scouting biodistribution of the therapeutic radiometals ^{90}Y and ^{177}Lu in tumor-bearing nude mice after coupling to the internalizing antibody cetuximab. J. Nucl. Med. 2005; 46:1898–1906. [PubMed: 16269605]

[37]. Aerts HJ, Dubois L, Perk L, Vermaelen P, van Dongen GA, Wouters BG, Lambin P. Disparity between in vivo EGFR expression and ^{89}Zr-labeled cetuximab uptake assessed with PET. J. Nucl. Med. 2009; 50:123–131. [PubMed: 19091906]

[38]. Pines G, Kostler WJ, Yarden Y. Oncogenic mutant forms of EGFR: lessons in signal transduction and targets for cancer therapy. FEBS Lett. 2010; 584:2699–2706. [PubMed: 20388509]

[39]. Yeh HH, Ogawa K, Balatoni J, Mukhapadhyay U, Pal A, Gonzalez-Lepera C, Shavrin A, Soghomonyan S, Flores L 2nd, Young D, Volgin AY, Najjar AM, Krasnykh V, Tong W, Alauddin MM, Gelovani JG. Molecular imaging of active mutant L858R EGF receptor (EGFR) kinase-expressing nonsmall cell lung carcinomas using PET/CT. Proc. Natl. Acad. Sci. USA. 2011 Epub.

[40]. Olson WC, Heston WD, Rajasekaran AK. Clinical trials of cancer therapies targeting prostate-specific membrane antigen. Rev. Recent Clin. Trials. 2007; 2:182–190. [PubMed: 18474004]

[41]. Manyak MJ. Indium-111 capromab pendetide in the management of recurrent prostate cancer. Expert Rev. Anticancer Ther. 2008; 8:175–181. [PubMed: 18279057]

[42]. Holland JP, Divilov V, Bander NH, Smith-Jones PM, Larson SM, Lewis JS. ^{89}Zr-DFO-J591 for immunoPET of prostate-specific membrane antigen expression in vivo. J. Nucl. Med. 2010; 51:1293–1300. [PubMed: 20660376]

[43]. Ruggiero A, Holland JP, Lewis JS, Grimm J. Cerenkov luminescence imaging of medical isotopes. J. Nucl. Med. 2010; 51:1123–1130. [PubMed: 20554722]

[44]. Webb DS, Shimizu Y, Van Seventer GA, Shaw S, Gerrard TL. LFA-3, CD44, and CD45: physiologic triggers of human monocyte TNF and IL-1 release. Science. 1990; 249:1295–1297. [PubMed: 1697984]

[45]. Jacobson K, O'Dell D, Holifield B, Murphy TL, August JT. Redistribution of a major cell surface glycoprotein during cell movement. J. Cell Biol. 1984; 99:1613–1623. [PubMed: 6386823]

[46]. Nestor M, Andersson K, Lundqvist H. Characterization of ^{111}In and ^{177}Lu-labeled antibodies binding to CD44v6 using a novel automated radioimmunoassay. J. Mol. Recognit. 2008; 21:179–183. [PubMed: 18438972]

[47]. Mulder JW, Kruyt PM, Sewnath M, Oosting J, Seldenrijk CA, Weidema WF, Offerhaus GJ, Pals ST. Colorectal cancer prognosis and expression of exon-v6-containing CD44 proteins. Lancet. 1994; 344:1470–1472. [PubMed: 7526103]

[48]. Heider KH, Kuthan H, Stehle G, Munzert G. CD44v6: a target for antibody-based cancer therapy. Cancer Immunol. Immunother. 2004; 53:567–579. [PubMed: 14762695]

[49]. Colnot DR, Quak JJ, Roos JC, van Lingen A, Wilhelm AJ, van Kamp GJ, Huijgens PC, Snow GB, van Dongen GA. Phase I therapy study of ^{186}Re-labeled chimeric monoclonal antibody U36 in patients with squamous cell carcinoma of the head and neck. J. Nucl. Med. 2000; 41:1999–2010. [PubMed: 11138685]

[50]. Colnot DR, Ossenkoppele GJ, Roos JC, Quak JJ, de Bree R, Borjesson PK, Huijgens PC, Snow GB, van Dongen GA. Reinfusion of unprocessed, granulocyte colony-stimulating factor-stimulated whole blood allows dose escalation of ^{186}Relabeled chimeric monoclonal antibody U36 radioimmunotherapy in a phase I dose escalation study. Clin. Cancer Res. 2002; 8:3401–3406. [PubMed: 12429627]

[51]. de Bree R, Roos JC, Plaizier MA, Quak JJ, van Kamp GJ, den Hollander W, Snow GB, van Dongen GA. Selection of monoclonal antibody E48 IgG or U36 IgG for adjuvant radioimmunotherapy in head and neck cancer patients. Br. J. Cancer. 1997; 75:1049–1060. [PubMed: 9083342]

[52]. Verel I, Visser GW, Boerman OC, van Eerd JE, Finn R, Boellaard R, Vosjan MJ, Stigter-van Walsum M, Snow GB, van Dongen GA. Long-lived positron emitters zirconium-89 and iodine-124 for scouting of therapeutic radioimmunoconjugates with PET. Cancer Biother. Radiopharm. 2003; 18:655–661. [PubMed: 14503961]

[53]. Borjesson PK, Jauw YW, de Bree R, Roos JC, Castelijns JA, Leemans CR, van Dongen GA, Boellaard R. Radiation dosimetry of ^{89}Zr-labeled chimeric monoclonal antibody U36 as used for immuno-PET in head and neck cancer patients. J. Nucl. Med. 2009; 50:1828–1836. [PubMed: 19837762]

[54]. Cai W, Chen X. Multimodality imaging of vascular endothelial growth factor and vascular endothelial growth factor receptor expression. Front. Biosci. 2007; 12:4267–4279. [PubMed: 17485373]

[55]. Ellis LM, Hicklin DJ. VEGF-targeted therapy: mechanisms of anti-tumour activity. Nat. Rev. Cancer. 2008; 8:579–591. [PubMed: 18596824]

[56]. Middleton G, Lapka DV. Bevacizumab (Avastin). Clin. J. Oncol. Nurs. 2004; 8:666–669. [PubMed: 15637962]

[57]. Nagengast WB, de Vries EG, Hospers GA, Mulder NH, de Jong JR, Hollema H, Brouwers AH, van Dongen GA, Perk LR, Lub-de Hooge MN. In vivo VEGF imaging with radiolabeled bevacizumab in a human ovarian tumor xenograft. J. Nucl. Med. 2007; 48:1313–1319. [PubMed: 17631557]

[58]. Nagengast WB, de Korte MA, Oude Munnink TH, Timmer-Bosscha H, den Dunnen WF, Hollema H, de Jong JR, Jensen MR, Quadt C, Garcia-Echeverria C, van Dongen GA, Lub-de

Hooge MN, Schroder CP, de Vries EG. ^{89}Zr-bevacizumab PET of early antiangiogenic tumor response to treatment with HSP90 inhibitor NVP-AUY922. J. Nucl. Med. 2010; 51:761–767. [PubMed: 20395337]

[59]. Swietach P, Hulikova A, Vaughan-Jones RD, Harris AL. New insights into the physiological role of carbonic anhydrase IX in tumour pH regulation. Oncogene. 2010; 29:6509–6521. [PubMed: 20890298]

[60]. Hoeben BA, Kaanders JH, Franssen GM, Troost EG, Rijken PF, Oosterwijk E, van Dongen GA, Oyen WJ, Boerman OC, Bussink J. PET of hypoxia with ^{89}Zr-labeled cG250-F(ab')$_2$ in head and neck tumors. J. Nucl. Med. 2010; 51:1076–1083. [PubMed: 20554724]

[61]. Heskamp S, van Laarhoven HW, Molkenboer-Kuenen JD, Franssen GM, Versleijen-Jonkers YM, Oyen WJ, van der Graaf WT, Boerman OC. ImmunoSPECT and immunoPET of IGF-1R expression with the radiolabeled antibody R1507 in a triple-negative breast cancer model. J. Nucl. Med. 2010; 51:1565–1572. [PubMed: 20847162]

[62]. Cai W, Chen X. Nanoplatforms for targeted molecular imaging in living subjects. Small. 2007; 3:1840–1854. [PubMed: 17943716]

[63]. Hong H, Gao T, Cai W. Molecular imaging with single-walled carbon nanotubes. Nano Today. 2009; 4:252–261. [PubMed: 21754949]

[64]. Ruggiero A, Villa CH, Holland JP, Sprinkle SR, May C, Lewis JS, Scheinberg DA, McDevitt MR. Imaging and treating tumor vasculature with targeted radiolabeled carbon nanotubes. Int. J. Nanomedicine. 2010; 5:783–802. [PubMed: 21042424]

[65]. Jacobson O, Zhu L, Niu G, Weiss ID, Szajek LP, Ma Y, Sun X, Yan Y, Kiesewetter DO, Liu S, Chen X. MicroPET imaging of integrin $\alpha_v\beta_3$ expressing tumors using ^{89}Zr-RGD peptides. Mol. Imaging Biol. 2011 Epub.

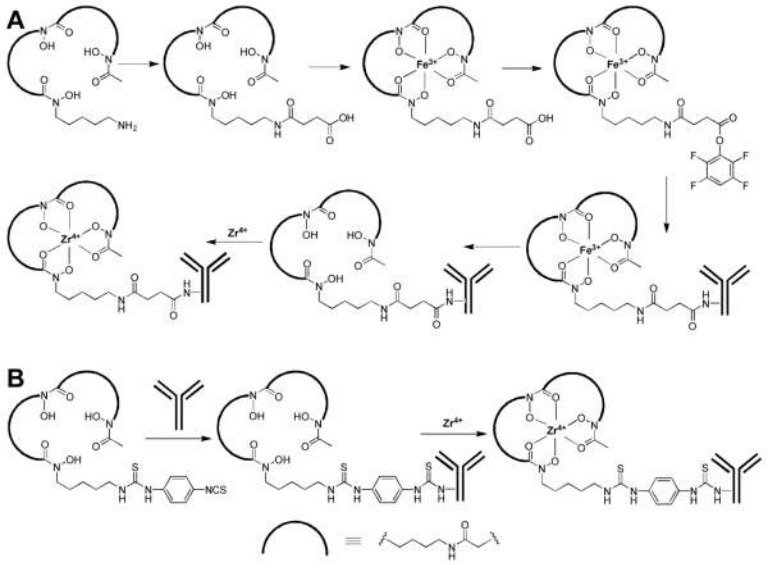

Fig. (1).
Representative radiochemistry for ^{89}Zr-labeling. (**A**) The 6-step route. (**B**) The 2-step method.

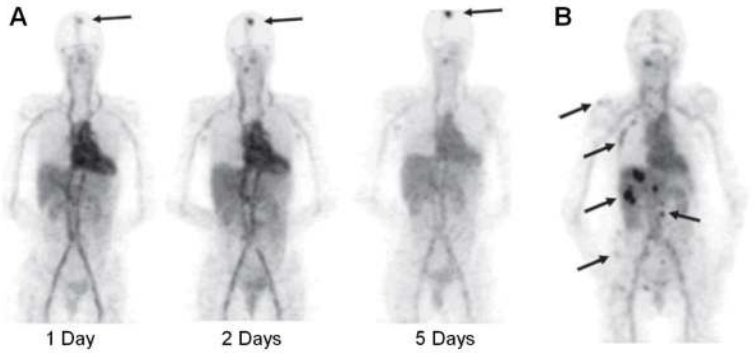

Fig. (2).
PET imaging of HER2 expression in patients with ^{89}Zr-trastuzumab. (**A**) ^{89}Zr-trastuzumab PET scans of a patient already on trastuzumab treatment at different time points post-injection revealed an increase over time in the tumor-to-nontumor ratio of tracer uptake. Arrow indicates ^{89}Zr-trastuzumab uptake in the only lesion. (**B**) ^{89}Zr-trastuzumab PET of a patient with liver and bone metastases at 5 days post-injection. A number of lesions are indicated by arrows. Adapted from [30].

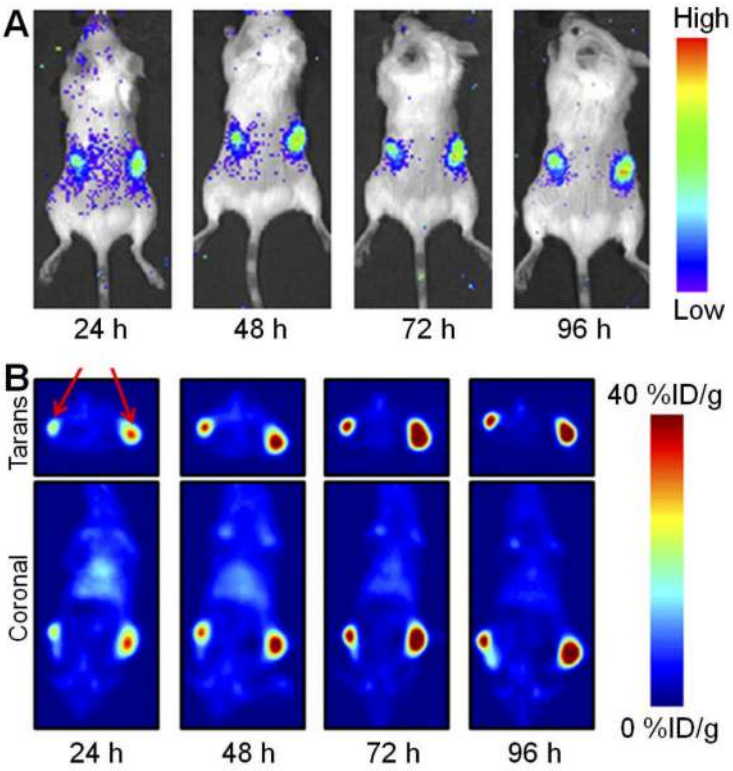

Fig. (3).

Multimodality imaging of PSMA with ^{89}Zr-J591. (**A**) Cerenkov luminescence imaging of tumor-bearing mice injected with ^{89}Zr-J591 in a small animal optical scanner. (**B**) Corresponding coronal and transverse immunoPET images of the mouse. The signal originates from the LNCaP tumors (PSMA-positive). Mouse bearing two different sized tumors of the same origin was used to demonstrate that differential uptake between the small and large tumors can be discerned by Cerenkov luminescence imaging. Adapted from [43].

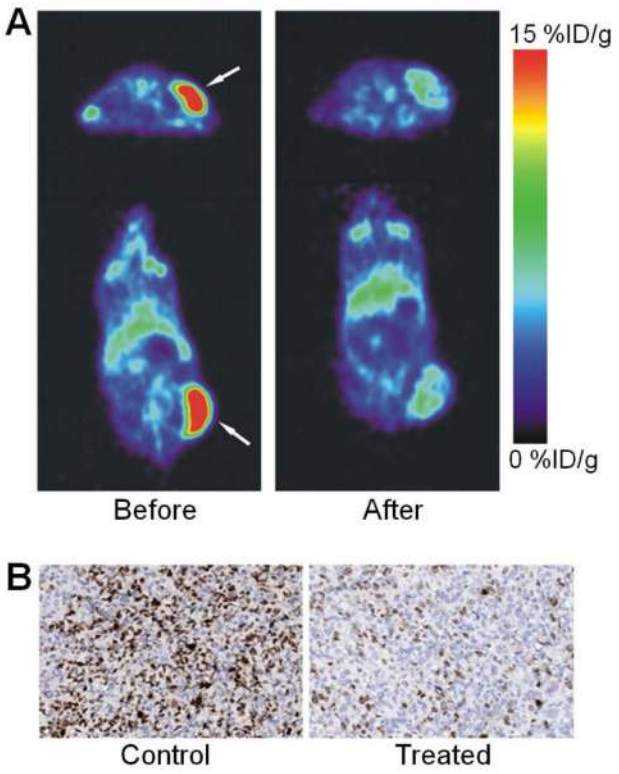

Fig. (4).
PET imaging of VEGF expression. (**A**) Transversal (top) and coronal (bottom) PET images of ^{89}Zr-bevacizumab in xenograft mice before (left) and after (right) treatment with a Hsp90 inhibitor. Arrows indicate the tumor. (**B**) Ki67 staining of the tumor tissue corroborated the PET results. Adapted from [58].